Characterization of Heat Loads from Mitigated Upward or Downward VDEs in DIII-D

E.M. Hollmann[1], N. Commaux[2], N.W. Eidietis[3],
C.J. Lasnier[4], R.A. Moyer[1], P.B Parks[3], and D. Shiraki[2]

[1]*University of California San Diego, 9500 Gilman Dr., La Jolla, CA 92093-0417, USA*
[2]*Oak Ridge National Laboratory, PO Box 2008, Oak Ridge, TN 37831, USA*
[3]*General Atomics, PO Box 85608, San Diego, California 92186-5608, USA*
[4]*Lawrence Livermore National Laboratory, Livermore, CA 94550, USA*

Experiments were conducted on the DIII-D tokamak to study vertically unstable plasma (VDE) disruption heat loads when mitigated with massive gas injection (MGI). MGI was performed with neon gas injection from dominantly either above or below the plasma. This was motivated by the present ITER plan to perform disruption thermal quench (TQ) mitigation mostly using valves located above the plasma, causing concern that downward VDEs could be poorly mitigated as a result. However, analysis of localized wall heat loads from IR camera images and radiated power from fast or slow bolometers shows no systematic difference in mitigation effectiveness of upper compared to lower gas valves, regardless of initial impurity injection location. This indicates that TQ mixing of impurities is faster than VDE timescales, resulting in TQ mitigation with similar global effectiveness for upper or lower MGI valve location.

The experiments presented here were performed in the DIII-D tokamak [1]. The target plasmas were an "ITER-like" shape with low triangularity and lower single null. At t = 2000 ms, the vertical stabilization system was turned off and the plasma was given a downward (or upward) kick with the shaping coils. The elongated plasma then goes vertically unstable, drifting into the lower (or upper) divertor. In the absence of mitigation, these plasmas go into a disruption thermal quench (TQ) around time t = 2025 ms. Mitigation is performed here with massive gas injection (MGI) of neon gas. MGI is done from two different locations: an "R+1" port located above the plasma at toroidal angle $\phi = 15°$ and an "R-2" port located below the plasma at toroidal angle $\phi = 135°$. MGI used 300 Torr-L of neon in a pulse about 1.5 ms long (at the valve).

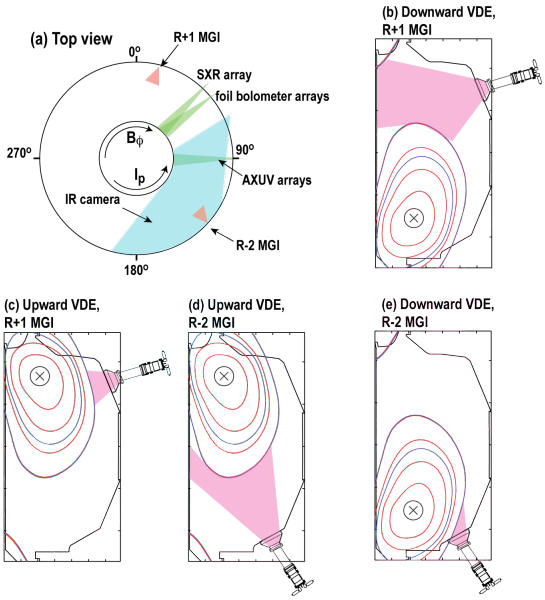

Fig. 1. (a) Overview of principal diagnostics and (b)-(e) schematics of different VDE directions/MGI location combinations.

Figure 1 gives: (a) an overview of principal diagnostics used here and (b) – (e) cartoons of the different mitigation combinations studied here

(downward VDE mitigated by R+1 MGI, upward VDE mitigated by R+1 MGI, upward VDE mitigated by R-2 MGI, and downward VDE mitigated by R-2 MGI). The core thermal collapse timing is dominantly diagnosed with soft x-ray arrays. Radiated power is measured with (fast) AXUV photodiode arrays and (slow) foil bolometer arrays. Wall heat loads are measured with a mid-IR (3-5 μm) camera.

An example of time traces from a VDE mitigated with R-2 MGI are shown in Fig. 2. In this shot, neon MGI is fired into the plasma before the VDE has caused the plasma to limit on the divertor and begin the TQ. The MGI "first light" impact of neon on the plasma edge occurs at t = 2017.2 ms. A rise in radiated power is observed, Fig. 2(g), and 1 ms later the plasma begins the TQ with the core temperature collapsing, Fig. 2(h). The mitigation "timeliness" is characterized by Δt_{MGI}, the delay between the MGI impact on the plasma edge and the expected TQ onset time if MGI had not been pre-emptively deployed.

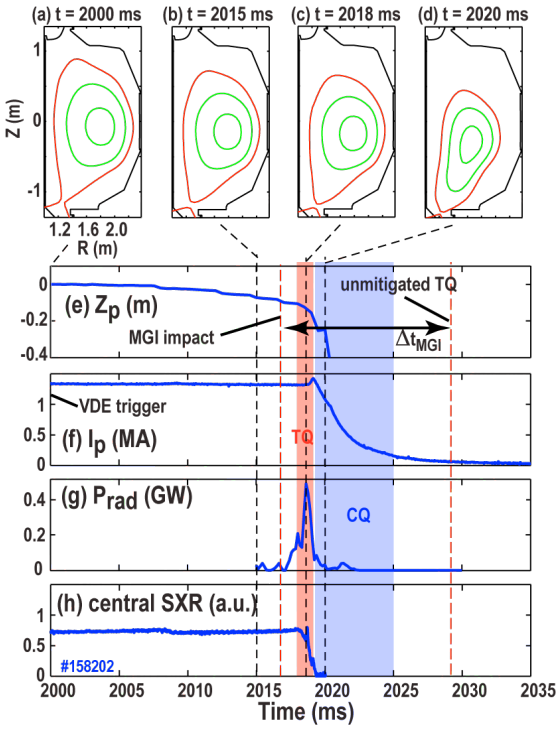

Fig. 2. Overview of mitigated VDE experiment time traces showing (a)-(d) JFIT reconstructions of magnetic flux surfaces, (e) vertical position, (f) plasma current, (g) radiated power, (h) central SXR.

Wall heat loads are measured with the DIII-D tangential IR camera [2]. The camera is kept to its full field of view during these experiments, thus covering much of the plasma cross section, but limiting the acquisition rate to 8 ms per frame. Because this acquisition rate is slower than the TQ duration (~ 2 ms), the temperature decay of the post-disruption images is used to estimate the time-averaged TQ heat flux to the walls. In the analysis, the temperature decay at each pixel is fit as a function of time after the disruption is over, assuming a separable contribution from the initial temperature of the surface (due to steady-state plasma heating) plus the contribution from the disruption heat pulse. Heat diffusion into a

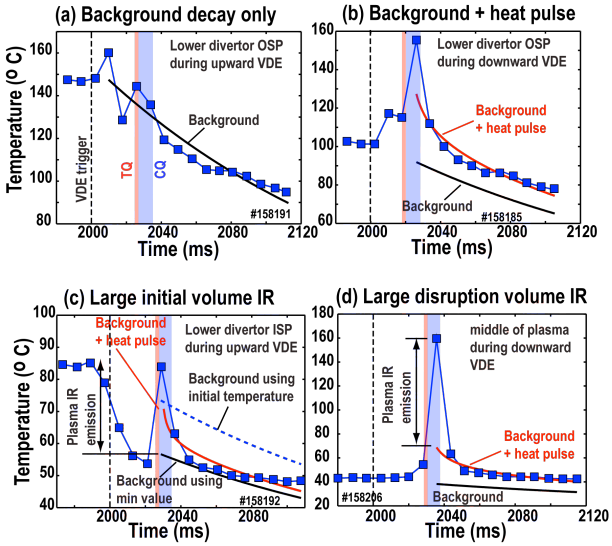

Fig. 3. Examples of fits to post-disruption IR data time sequences at different locations showing: (a) background temperature decay in location with negligible disruption heating, (b) total temperature decay in location with comparable initial and disruption heat pulse heating, (c) temperature decay fits in location with significant initial plasma IR emission, and (d) temperature decay fits in location with significant disruption plasma IR emission.

semi-infinite plane is assumed [3]. Blackbody radiation, lateral heat diffusion, and variation of wall properties with temperature are ignored. The background temperature cooling time constant τ_∞ is fit experimentally from lower divertor pixels after upward VDEs, where initial heating dominates. Typically, $\tau_\infty \approx 170$ ms is found, as shown in Fig. 3(a). A sample fit where both initial wall temperature and disruption heat pulse are significant is shown in Fig. 3(b). In some pixels, volume plasma IR emission prior to the disruption is significant; an example of this is shown in Fig. 3(c). This is corrected for by lowering the initial temperature T_0 until the background decay curve lies below all data points. To avoid volume IR emission during the disruption, fits are performed only on data points past the end of the CQ. Frequently, the data point(s) falling during the CQ time window are observed to lie well above the fit; this is interpreted as being at least partially due to volume IR emission during the CQ. An example of this is shown in Fig. 3(d), where a very large deviation from the post-disruption decay fit is seen during the CQ.

Figure 4 shows an example of IR images and resulting reconstructed disruption heat flux for an unmitigated upward VDE. Figure 4(a) gives an example pre-disruption IR image, Fig. 4(b) shows a during-disruption IR image, and Fig. 4(c) shows an image of the resulting calculated disruption heat flux. Figure 4(d) shows a CAD model of the IR camera view.

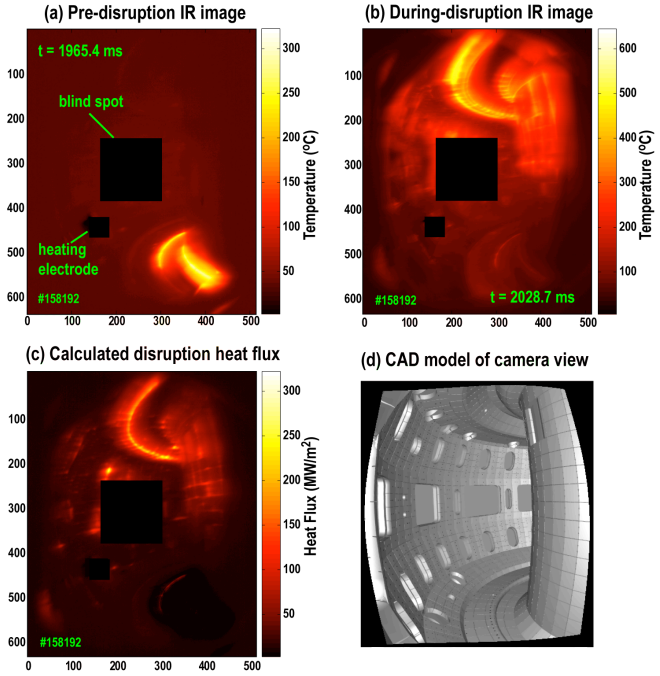

Fig. 4. Example IR images for an unmitigated upward VDE showing: (a) pre-disruption image, (b) during-disruption image, (c) calculated disruption heat flux, and (d) CAD model of IR camera view.

Figure 5 gives an overview of 0D trends in effectiveness of MGI mitigation of VDEs. The data are plotted as a function of the MGI impact delay Δt_{MGI}. Figure 5(a) shows the total radiated energy estimated by tomography of the slow bolometers. Figure 5(b) shows the energy going into localized wall heating estimated from IR images and assuming toroidal symmetry (this includes both conducted and convected contributions). Figure 5(c) shows vertical vessel motion, giving a qualitative picture of vessel forces. Figure 5(d) gives the magnitude of the plasma current decay rate. This gives a rough picture of the amount of impurities in the CQ plasma, with larger impurity levels giving a lower temperature and a faster current decay rate. The data with $\Delta t_{MGI} = 5$ ms actually corresponds to unmitigated VDE disruptions with no MGI.

Figure 5 indicates that there is no significant global improvement in mitigation effectiveness of VDEs when using a MGI port closer to the VDE direction. In contrast, MGI timing delay Δt_{MGI} clearly has a large effect, with earlier MGI resulting in higher radiated energies, lower localized heat fluxes, and lower vessel motion. Even injecting during the TQ ($\Delta t_{MGI} = 0$) appears to have some small mitigation benefit over not using MGI at all. This data thus suggests that TQ mixing of heat and impurities is very effective even when the plasma is limited on the divertor. This effective TQ mixing tends to smooth out the effect of injection location on global disruption mitigation indicators. One trend in the data which is not understood at present, is the large difference in heat loads seen between upward and downward VDEs, Fig. 5(b). This may be due to upper and lower divertor surfaces having different material properties, such as IR emissivity.

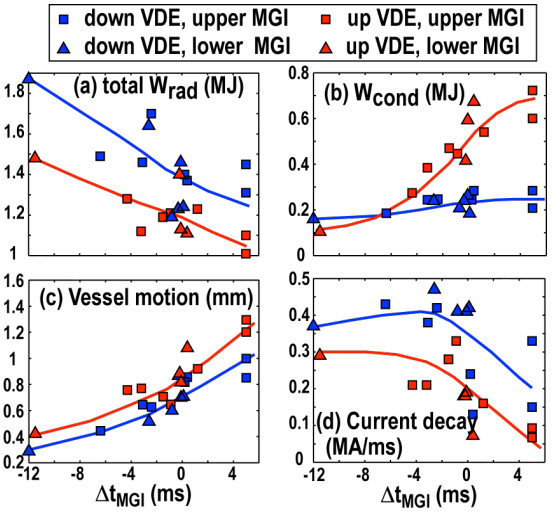

Fig. 5. Global trends in VDE mitigation effectiveness for different VDE direction/MGI location combinations as a function of MGI trigger delay Δt_{MGI} showing (a) total radiated energy, (b) total conducted/convected energy, (c) vessel vertical motion, and (d) CQ current decay rate.

This material is based upon work supported by the U.S. Department of Energy, Office of Science, Office of Fusion Energy Sciences, using the DIII-D National Fusion Facility, a DOE Office of Science user facility, under Awards DE-FG02-07ER54917, DE-FC02-04ER54698, DE-AC05-00OR22725, DE-AC52-07NA27344, and DE-AC05-06OR23100. DIII-D data shown in this paper can be obtained in digital format by following the links at https://fusion.gat.com/global/D3D_DMP.

[1] J. L. Luxon, Nucl. Fusion **42** (2002) 614.
[2] C.J. Lasnier, et al., Rev. Sci. Instrum. **85**, 11D855 (2014).
[3] H.S. Carslow and J.C. Jaeger, Conduction of Heat in Solids, 2nd Ed. (Oxford, Claredon, 1995).